A crucial role of land-atmosphere interactions in shaping subseasonal convective variability over the Maritime Continent in idealized model simulations

Xianan Jiang[1,2*] and Hsi-Yen Ma[3]

[1]Joint Institute for Regional Earth System Science and Engineering, University of California, Los Angeles, California, USA

[2]Jet Propulsion Laboratory, California Institute of Technology, Pasadena, California, USA

[3]Lawrence Livermore National Laboratory, Livermore, California, USA

Submitted to *J. Climate,* November 2025

Revised, April 2026

Accept, September 2026

Corresponding author address: Dr. Xianan Jiang, Jet Propulsion Laboratory, California Institute of Technology, MS 233-300, 4800 Oak Grove Drive, Pasadena, CA 91109. Email: xianan@ucla.edu.

Abstract

The limitations of current Earth system models in accurately representing the propagation of the Madden-Julian Oscillation (MJO) over the Maritime Continent (MC) significantly hinder our ability to make skillful subseasonal-to-seasonal predictions of extreme weather events worldwide. Additionally, our understanding of the intricate interactions between the MJO and the MC remains incomplete. Focusing specifically on Sumatra Island, this study investigates the key processes underlying the damping effect of MC islands on the eastward-propagating MJO based on a series of idealized atmospheric-only global model simulations, which include realistic land-sea distributions and topography of the MC within an aqua-planet environment. The findings suggest that the coupling between land and atmosphere, driven by interactions among clouds, radiation, land surface temperature, and convective instability, plays a critical role in reducing MJO convection over the MC. Notably, incorporating the diurnal cycle of convection in the model significantly enhances this damping effect, due to more active interactions between convection and radiation, consistent with previous modeling studies.

1. Introduction

Due to its widespread influences on global weather patterns, the Madden-Julian Oscillation (MJO) serves as one of the most important sources of predictability for subseasonal-to-seasonal predictions of extreme climate and weather events (Balmaseda et al. 2020; Jiang et al. 2020b; Merryfield et al. 2020). Over the past few decades, significant community efforts have been devoted to improving the understanding of the essential physics and the prediction skill of the MJO, e.g., through coordinated international field campaigns and modeling projects (e.g., Moncrieff et al. 2012; Yoneyama et al. 2013; Jiang et al. 2015; Neena et al. 2014; Pegion et al. 2019; Yoneyama and Zhang 2020; see Jiang et al. 2020b for a review). Despite these advancements, MJO prediction skill remains limited in current climate and weather forecasting models, with a typical useful lead time of 3–5 weeks (e.g., H. Kim et al., 2018; Jiang et al. 2020b), falling short of its estimated intrinsic potential predictability of about 5–7 weeks (e.g., Neena et al., 2014).

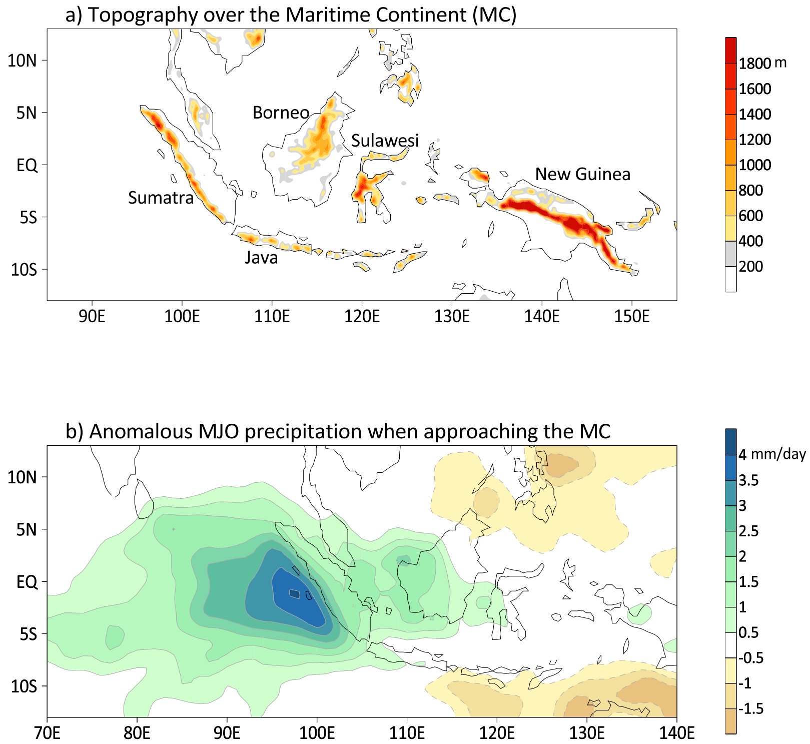

Fig. 1. a) Surface elevation over the Maritime Continent (units: m). b) Spatial pattern of precipitation anomalies associated with the MJO as it approaches the MC during its eastward propagation from the Indian Ocean. This precipitation pattern is derived from a composite analysis over multiple MJO events using the GPM precipitation dataset. See text for details regarding the composite methodology.

One key process limiting the predictive skill of the MJO is the deficiency of current climate models in accurately representing the interactions between the MJO and tropical landmasses, particularly over the Maritime Continent (MC). In this region, the presence of steep mountains (Figure 1a) adds complexity to the development of MJO convection (Kim et al. 2020; Jiang et al. 2020b). The MC often acts as a barrier to the eastward propagation of the MJO from the Indian Ocean to the western Pacific (e.g., Salby and Hendon 1994; Kim et al. 2014; Ling et al. 2019), with about 40% of observed MJO events dissipating over the MC region (Kerns and Chen 2020). This "MC barrier effect" on the eastward propagating MJO is clearly evident in satellite observations, as illustrated in Figure 1b. As the MJO approaches the MC, significant precipitation is primarily concentrated over the eastern Indian Ocean, off the west coast of Sumatra Island, while precipitation amplitude is notably weaker over the land region. The interactions between the MJO and the MC are not yet fully understood and remain poorly simulated in current climate models, including high-resolution cloud-resolving models (e.g., Love et al., 2011; Peatman et al., 2015; Birch et al., 2016; Hagos et al., 2016). As a result of these limitations, models struggle to predict the MJO and its downstream impacts, such as tropical cyclone genesis over the western and eastern Pacific, as well as MJO-induced extratropical Rossby-wave teleconnection patterns (e.g., Peatman et al. 2015; Birch et al. 2016; Baranowski et al. 2019; Vitart 2016; Kim et al. 2019; Wang et al. 2020; Abhik et al. 2023).

Various local and large-scale processes have been proposed to explain the MC barrier effect on MJO propagation. Early studies suggest that the steep topography over the major MC islands (Fig. 1a) plays a critical role in the weakening of MJO convection (Hsu and Lee 2005; Inness and Slingo 2006; Wu and Hsu 2009). This weakening is primarily attributed to the lifting and frictional effects of the orography, which interrupts the development of anomalous low-level circulation, which is critical for triggering new convection eastward of the primary MJO convective envelope.

As surface latent heat fluxes serve as the primary energy source in sustaining MJO convective instability (e.g., Maloney and Sobel 2004; Kim et al. 2011; Maloney 2009; Andersen and Kuang 2012; Jiang 2017), the damping of MJO convection over MC land may result from a lack of moist energy supply by surface latent heat fluxes due to limited moisture-holding capacity over land (e.g., Maloney and Sobel 2004; Sobel et al. 2008; Sobel et al. 2010). Furthermore, in contrast to oceanic regions where surface fluxes are mainly driven by MJO convection-induced surface wind anomalies, surface turbulent fluxes over the tropical rainforests of the MC region are primarily governed by transpiration, which is strongly dependent on incoming solar radiation rather than winds. This fundamental difference can potentially decouple MC convection from the large-scale circulation, thereby weakening the MJO over the MC (Lee et al. 2012).

The reduced MJO amplitude over the MC has also been ascribed to upscale influences from high-frequency convective systems over this region, particularly the vigorous diurnal cycle resulting from surface solar heating and associated sea- and land-breeze circulations. A prominent hypothesis regarding how the diurnal cycle influences the MJO is through the competition for moist static energy between diurnal convection and low-frequency variability (e.g., Wang and Li 1994; Zhang and Hendon 1997; Neale and Slingo 2003; Oh et al. 2012; Oh et al. 2013). Vigorous diurnal rainfall variability over MC land tends to consume the moist energy available to support MJO convection, while simultaneously suppressing the development of mesoscale convective systems (MCSs) over the ocean - a process critical for MJO propagation over the MC region (Zhang and Ling 2017; Ling et al. 2019). The damping of MJO convection by a strong diurnal cycle over the MC is supported by several modeling studies (e.g., Oh et al. 2013; Hagos et al. 2016; Majda and Yang 2016; Ahn et al. 2020a), although the precise processes underlying this cross-scale interaction remain elusive.

Recent analyses of MJO moisture and moist static energy (MSE) processes over the MC suggest that the topographically phase-locked mean moisture pattern over the MC, with moisture maxima collocated with local mountain peaks, plays a key role in the disruption of MJO convection east of the MC mountains via a drying effect driven by horizontal moisture advection (Hung and Sui 2018; Jiang et al. 2019). Specifically, over Sumatra, a belt of mountain peaks is situated along the west coast of the island and straddles the equator between 5^{o}S and 5^{o}N (Fig. 1a). This orographic setting can effectively lead to the weakening of MJO convection over a large portion of the island east of the mountains.

In addition to local processes, MJO propagation over the MC can also be subject to strong modulation by the large-scale environment over the Indo-Pacific warm pool. Recent studies suggest that the horizontal advection of background lower-tropospheric moisture or MSE by the anomalous MJO circulation plays a dominant role in MJO propagation over the Indo-Pacific warm pool (e.g., Maloney 2009; Andersen and Kuang, 2012; Kim et al., 2014; Sobel et al. 2014; Chikira 2014; Adames and Wallace 2015; Kim et al. 2017; Jiang 2017; Gonzalez and Jiang 2019). The MJO circulation exhibits a distinct east-west asymmetry, characterized by easterly Kelvin wave responses to the east and westerly Rossby wave responses to the west of the main convection. Concurrently, the seasonal mean moisture pattern over the Indo-Pacific warming pool features a maximum center near the MC. This configuration, with a positive zonal mean moisture gradient over the Indian Ocean, leads to moistening (drying) to the east (west) of MJO convection, thereby promoting its eastward propagation (Jiang 2017; Gonzalez and Jiang 2017; Kim 2017; Lim et al. 2018; Kim et al. 2019; Ahn et al. 2020b). This same mechanism, however, favors a weakening of the MJO eastward propagation or even a westward propagation on the eastern side of the warm pool (i.e., east of the MC), due to the reversal of the zonal mean moisture gradient. The prevalence of a westward-propagating intraseasonal mode is indeed observed over the western Pacific (Feng et al. 2015; DeMott et al. 2018; Gonzalez and Jiang 2019). These results suggest that the Indo-Pacific warm pool tends to trap the eastward-propagating MJO near the MC region, and whether the MJO successfully traverses the MC can be closely linked to the zonal shift of the Indo-Pacific warm pool, for example, in association with the variability of the El Niño. Additionally, cross-equatorial cold surges associated with off-equatorial systems can also strongly alter the regional circulation and moisture patterns, effectively disrupting or redirecting MJO convection around the MC (Kim et al. 2017; Xavier et al. 2020; Lubis et al. 2023).

Given the multitude of processes involved, it is difficult to identify the essential processes underlying the MC barrier effect on the MJO in the real word. In this study, by utilizing a series of idealized global climate model (GCM) simulations with a specific focus on local processes over Sumatra Island, we illustrate that the coupling between land and atmosphere, through interactions among clouds, radiation, land surface temperature, and convection, plays a crucial role in damping MJO convection over MC islands. Notably, this MC damping is effectively amplified by a temporal phase-locking mechanism among these local diurnal fields and the large-scale MJO envelope.

2. Model experiments, Observational dataset, and Methods

2.1 The global climate model and experimental design

The atmospheric GCM (AGCM) simulations analyzed in this study is based on the ECHAM AGCM version 4.6 (Roeckner et al. 1996). To better resolve development of convection over the MC region, a horizontal resolution of T106 (~ 1°) is applied for all experiments in this study, along with 19 vertical model levels. The model employs the mass flux convection scheme developed by Tiedtke (1989) for penetrative, shallow, and mid-level convection, with modifications by Nordeng (1994) that link the cloud-base mass flux to convective instability for the penetrative convection.

The land surface parameterization scheme in ECHAM4 accounts for the evolution of the soil temperature profile, soil hydrology, and snowpack over land. Soil temperature is determined via heat conduction across five layers (with thicknesses of 0.065, 0.254, 0.913, 2.902, and 5.70 m from top to bottom), using net surface heat fluxes as the upper boundary condition and a zero heat flux at a 10-m depth as the lower boundary condition. Soil moisture is computed based on a one-layer bucket model (Manabe 1969), with the field capacity varying by soil type. The governing equation for soil moisture incorporates precipitation, snowmelt, evaporation, runoff, and drainage. Direct evaporation of soil moisture from bare soil and wet vegetation canopies, as well as evapotranspiration via root uptake, are explicitly parameterized (Roeckner et al. 1996).

Following Jiang et al. (2020a), an idealized aqua-planet simulation is conducted to exclude complex influences from lower boundary conditions, including the land-sea contrast and orography. This model is forced by a zonally uniform sea surface temperature (SST) pattern with a latitudinal profile following Neale and Hoskins (2000) (Fig. 2a), defined as follows:

$$T_s = \begin{cases} 27^{o}\mathrm{C}\left(1 - 0.5 * sin^2\left(\frac{3\varphi}{2}\right) - 0.5 * sin^4\left(\frac{3\varphi}{2}\right)\right) & : -\frac{\pi}{3} < \varphi < \frac{\pi}{3} \\ 0^{o}\mathrm{C} & : \text{others} \end{cases} \quad (1)$$

where φ is latitude. This SST profile has been referred to as the “QOBS” profile, as it closely resembles the observed annual and zonal mean SST (Neale and Hoskins 2000). To focus on the eastward propagation of the MJO during the boreal winter season, we set the model solar radiation to the perpetual condition of March, when the maximum solar radiation is located near the equator. The model sea ice is set to zero, and aerosols are switched off. Otherwise, the default physics of ECHAM4.6 is used, explicitly retaining the diurnal changes in solar radiation.

As shown in Jiang et al. (2020a), this idealized aqua-planet AGCM simulation (hereafter, the “Control” experiment) successfully captures the systematic eastward propagation of intraseasonal convection along the equator, exhibiting typical characteristics of the observed MJO (see Fig. 2b). The simulated eastward propagation of intraseasonal convection is well explained by variations in moisture anomalies, consistent with the moisture mode theory of the MJO (Jiang et al. 2020a; Adames and Maloney 2021).

Building upon the successful simulation of the eastward-propagating MJO in the “Control” experiment, a new experiment is conducted by embedding the MC islands into the aqua-planet environment (hereafter, the “MC” experiment; Fig. 2c). Land surface properties over the MC islands –including the land-sea mask, topography, vegetation types– are adopted from the standard ECHAM4.6 configuration. To isolate the topographic effect of the MC mountains on MJO convection, an additional experiment based on the experiment "MC" is conducted by flattening the orography over the MC land, while keeping other land surface properties unchanged (hereafter, the "MC_flat" experiment).

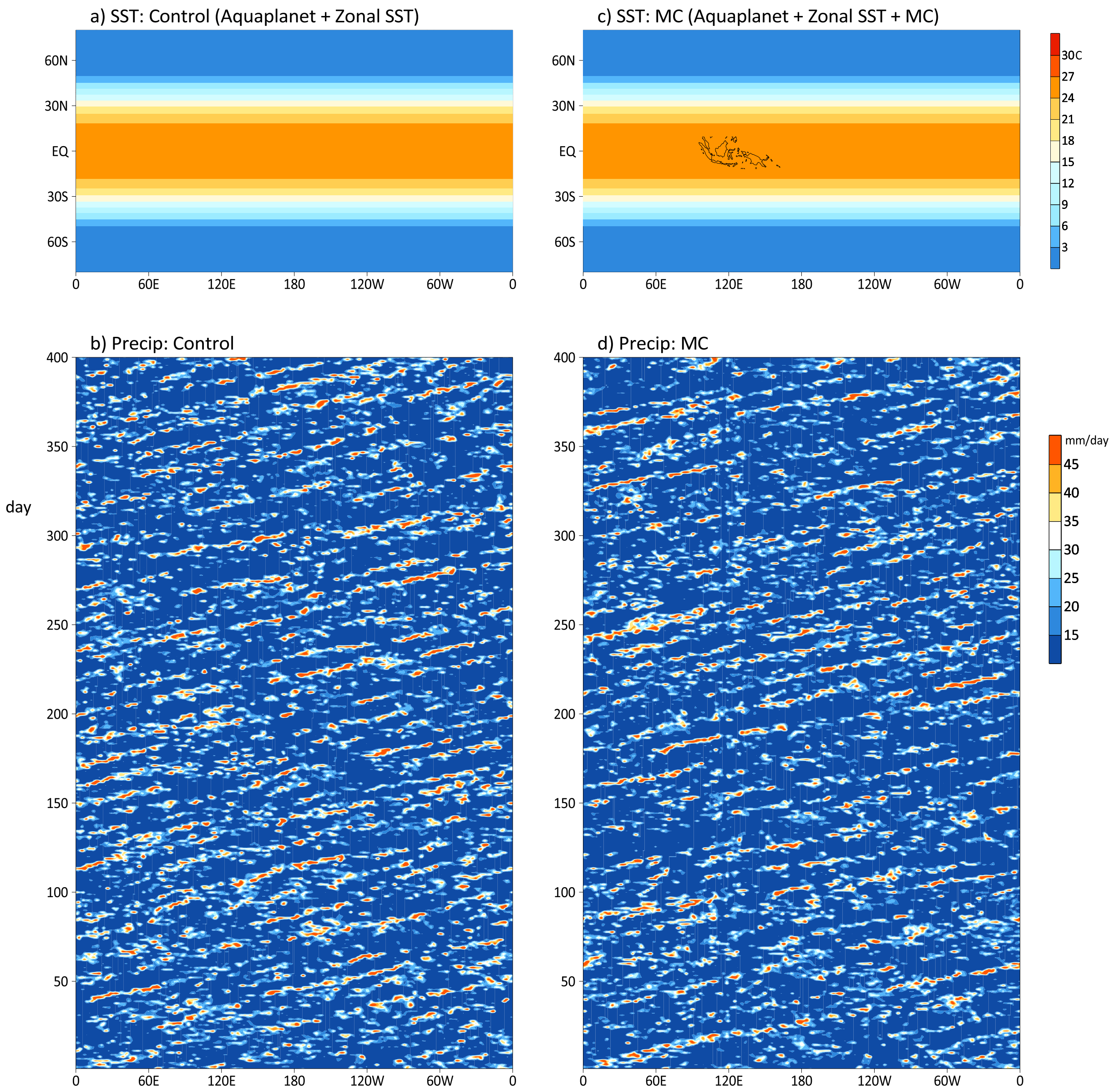

Fig. 2. a) Spatial distribution of the zonally uniform sea surface temperature pattern used as the lower boundary forcing in the "Control" experiment based on the ECHAM AGCM; b) A snapshot of the longitude-time evolution of rainfall along the equator, averaged over 7.5°S–7.5°N (units: mm day^{-1}), in the "Control" experiment. c) As in a), but for the "MC" experiment with a realistic land configuration over the MC region embedded in the aqua-planet environment. d) As in b), but for the rainfall evolution in the "MC" experiment.

The role of the diurnal cycle in the interactions between the MJO and MC land is further examined by turning off the diurnal variations of solar radiation. Specifically, the time-varying solar zenith angle and day length at each grid point are replaced by the mean daytime solar zenith angle and the fractional day length for the corresponding latitude, effectively applying a daily mean insolation at each grid point along that latitude (the "MC_flat_nodiurnal" experiment). As will be discussed later, these experiments suggest that the land-atmosphere coupling, as essentially captured in the "MC_flat" experiment, plays a critical role in the MC barrier effect. Therefore, a series of additional experiments are conducted based on the "MC_flat" configuration to further identify the key land-atmosphere processes underlying the damping of MJO convection over the MC (Exps. 5-10 in Table 1, to be detailed in subsequent sections).

Benefiting from the perpetual March radiation conditions specified in these experiments, sensitivity tests indicate that the statistical characteristics of the MJO over the MC region derived from 5-year simulations are largely consistent with those from 10-year simulations. Therefore, the analyses presented in the subsequent sections are based on five consecutive years of integration after an initial spin-up period for each of the aforementioned experiments.

Table 1: Idealized AGCM experiments analyzed in this study

Exp. #	Experiment Name	Descriptions
1	Control	Global aqua-planet simulation with lower boundary SST forcing defined the Eq. (1).
2	MC	As in "Control" but with realistic land surface properties over the MC (including land-sea mask, topography, and vegetation types)
3	MC_flat	As in "MC", but with flattened topography over the MC land.
4	MC_flat_nodiurnal	As in "MC_flat", but with diurnal variations of solar radiation replaced by zonally-mean values (see text for details).
5	MC_flat_nocoupling	As in "MC_flat", but with land-atmosphere interactions turned off by overriding the model surface temperature (T_S) and soil moisture (W_S) with their climatological means from "MC_flat" at each model time step.
6	MC_flat_T_S_coupling	As in "MC_flat", but isolating Ts coupling by allowing Ts to freely evolve, while overriding W_S with its climatological mean from "MC_flat".
7	MC_flat_W_S_coupling	As in "MC_flat", but isolating Ws coupling by allowing Ws to freely evolve, while overriding T_S with its climatological mean from "MC_flat".
8	MC_flat_T_S_Q_R_coupling	As in "MC_flat_T_S_coupling", but restricting Ts variations to those driven solely by surface radiative fluxes (Q_R), while overriding surface latent and sensible heat fluxes (F_S) and W_S with their climatological means from "MC_flat".
9	MC_flat_T_S_F_S_coupling	As in "MC_flat_T_S_coupling", but restricting Ts variations to those driven solely by F_S, while overriding Q_R and W_S with their climatological means from "MC_flat".
10	MC_flat_T_S_Q_R_coupling_nodiurnal	As in "MC_flat_T_S_Q_R_coupling", but with the diurnal cycle of solar radiation turned off (replaced by zonally-mean values).

2.2 Observational datasets

Rainfall observations from the Global Precipitation Measurement (GPM) mission's Integrated Multi-satellitE Retrievals for GPM (IMERG) product are used to characterize the diurnal precipitation evolution and MJO convection over the MC region, as well as to validate the model simulations. The GPM IMERG provides a global precipitation product by unifying observations from a network of partner satellites in the GPM constellation with high-resolution (0.1°), half-hourly precipitation estimates since 2000 (Huffman et al. 2019). For this study, hourly-averaged GPM rainfall observations spanning the period 2001-2023 are employed.

2.3 Identification of MJO signals over the MC region

To examine the influences of the MC on MJO convection in both observations and model simulations, we conduct composite analyses of precipitation anomalies for strong MJO events with their convection centers located over the eastern Indian Ocean, immediately west of Sumatra. A daily MJO index is defined by the 10-90-day band-pass filtered precipitation anomalies (after the removal of the climatological annual cycle, defined by the annual mean plus the first three harmonics) averaged over an eastern Indian Ocean box (5°S-5°N; 90°-100°E; see the blue box in Fig. 3a). The relatively broad 10–90-day frequency band is utilized here to fully capture the simulated MJO signals, which tend to exhibit a slightly higher frequency in the idealized aqua-planet framework compared to observations (Jiang et al. 2020a). The peak days of strong positive and negative MJO events over the eastern Indian Ocean are then identified by local maxima or minima in the MJO index that exceed +1 standard-deviation (STD) and fall below -1 STD, respectively.

For the model simulations, the MJO index is based on a 5-year integration (excluding the first three months to account for model spin-up), whereas for the GPM observations, it is derived for the extended boreal winter seasons (November to March) for the 2001-2023 period. The evolution of anomalous precipitation and other variables associated with the MJO over the eastern Indian Ocean can then be derived by averaging the 10-90-day filtered fields of these variables across the identified peak days. Since composites for positive and negative MJO events largely mirror each other with an opposite sign, we only show patterns associated with positive MJO events over the eastern Indian Ocean in the subsequent discussions, constructed by taking the difference between the positive and negative composites dividing by two. For example, Fig. 1b illustrates the anomalous precipitation pattern associated with the MJO events peaking over the eastern Indian Ocean based on GPM IMERG, derived from a composite over 43 positive and 41 negative MJO events during the boreal winter seasons from 2001-2023. For 5-year model simulations, typically about 60 strong positive and 60 strong negative MJO events are selected for the composite analyses.

3. Results

3.1 Representation of the MC barrier effect in idealized AGCM simulations

As reported in Jiang et al. (2020a), forced by the QOBS SST pattern, the aqua-planet ECHAM4.6 AGCM simulation in the “Control” experiment successfully captures the frequent occurrence of coherent eastward-propagating MJO events (Fig. 2b). These eastward-propagating convective events largely remain intact in the “MC” experiment (Fig. 2d), as the global mean state is not significantly altered by the inclusion of the MC landmasses due to their relatively small spatial extent (figure not shown). This experimental framework thus provides an excellent opportunity to investigate the interactions between the MJO and the MC islands under a realistic land-sea configuration. While a subtle interruption of the eastward-propagating convection over the MC region can be visually discerned in this Hovmöller snapshot (Fig. 2d), the detailed damping effect is more rigorously demonstrated through the composite analysis presented in Fig. 3. As previously discussed, the presence of the observed Indo-Pacific warm pool itself can exert a damping effect on the eastward propagation of the MJO near the MC. Therefore, by excluding the large-scale influences from the Indo-Pacific warm pool, the idealized zonally uniform QOBS SST pattern specified in the “MC” experiment makes it possible to cleanly isolate the local processes over the MC region that contribute to the MC barrier effect on the eastward-propagating MJO.

Based on the composite method for strong positive and negative MJO events as described earlier, Figures 3a and 3c illustrate the anomalous precipitation patterns associated with the MJO over the eastern Indian Ocean in the “Control” and “MC” experiments, respectively. Compared to that in the “Control” experiment (Fig. 3a), a significant modulation of MJO convection over the MC region is readily apparent in the “MC” experiment (Fig. 3c), closely resembling the anomalous precipitation pattern in the observations (Fig. 1b). Specifically, strong MJO precipitation anomalies are primarily concentrated over the eastern Indian Ocean off the west coast of Sumatra, while remaining notably weak over Sumatra itself. Given this realistic simulation of the observed MC barrier effect on the MJO in the “MC” experiment, further investigations based on this experiment will provide critical insights into the underlying physics responsible for the MC barrier effect. Since the sharp reduction of the MJO convection over Sumatra compared to the neighboring oceanic regions in the “MC” experiment is primarily driven by changes in convective precipitation (see Supporting Figure S1; compare Figs. 3b and 3d for the “Control” and “MC” experiments), the following analysis will mainly focus on the physical processes responsible for the damping of MJO convective precipitation over Sumatra.

3.2 The crucial role of land-atmosphere interactions in the MC barrier effect

To explore the potential role of the MC mountains in the MC barrier effect, an additional experiment, "MC_flat", is conducted based on the "MC" experiment but with flattened topography over the MC (Table 1). As shown in Figs. 3e and 3f, even with the flattened topography over MC, the strong damping of MJO precipitation anomalies over Sumatra is still well represented in the "MC_flat" experiment, closely resembling that simulated in the "MC" experiment. It is noteworthy that given the limitation of the model's ~1° horizontal resolution, the topographic effect of the MC mountains on MJO convection in reality might be underestimated in the "MC" experiment. However, the substantial damping of MJO convection captured in the "MC_flat" experiment strongly indicates that land-atmosphere interactions over the MC play a crucial role in the MC barrier effect on MJO convection.

The potential role of the diurnal variations in solar radiation in the MC barrier effect on the MJO is further examined in the "MC_flat_nodiurnal" experiment, which is based on "MC_flat" but with the diurnal variations of solar radiation replaced by its zonally averaged values. While an overall weakening of MJO convective precipitation over Sumatra is still evident in this experiment (Fig. 3h), the amplitude contrast of convective precipitation anomalies between Sumatra and the eastern Indian Ocean is notably reduced compared to that in the "MC_flat" experiment (to be further discussed below). This result is largely in accord with previous studies that highlight a potential role of the diurnal cycle in enhancing the damping of MJO convection over the MC (e.g., Oh et al. 2013; Hagos et al. 2016). Furthermore, the modulation of terrestrial precipitation through diurnal surface forcings aligns with recent findings on the critical role of island-scale cloud-radiative interactions (Najarian et al. 2025).

To quantify the relative contributions of land-atmosphere interactions, the MC topography, and the diurnal cycle to the total MC barrier effect, we develop an objective approach to measure the damping of MJO convection over Sumatra across different model simulations. Since the damping of MJO convection over the MC is mainly driven by changes in convective precipitation as previously discussed (Supporting Fig. S1), we calculate the ratio of MJO convective precipitation anomalies averaged over Sumatra (the red region in Fig. 3c) to those over the eastern Indian Ocean near the MJO convection center (the blue box region in Fig. 3a) in each simulation.

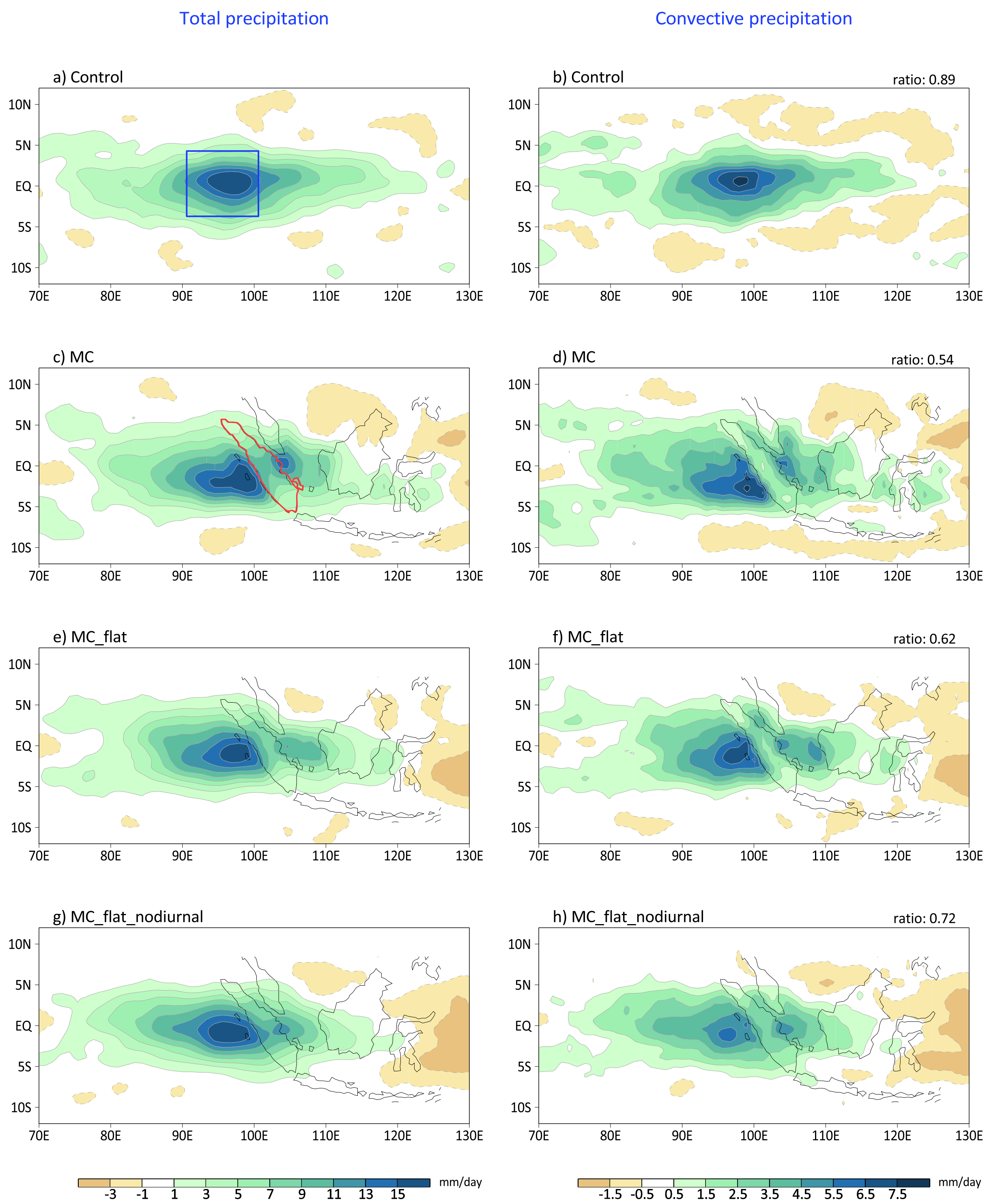

Fig. 3. As in Fig. 1b, but for the spatial patterns of total (left panels) and convective (right panels) precipitation anomalies in various AGCM simulations, including the "Control" (a, b), "MC" (c, d), "MC_flat" (e, f), and "MC_flat_nodiurnal" (g, h) experiments. These anomalous precipitation patterns are derived from composite analyses of multiple MJO events peaking over the eastern Indian Ocean. The value displayed in the upper right corner of each right panel denotes the corresponding convective precipitation ratio between Sumatra and the MJO convection center over the eastern Indian Ocean (see text for details). Note the different color scales for the total and convective precipitation anomalies.

For example, a ratio of 0.89 is obtained in the "Control" experiment (Fig. 3b). Given the absence of the MC land in this experiment, a ratio of less than 1 simply reflects the natural spatial decay of MJO convection away from its center. Corresponding ratios in the experiments of "MC", "MC_flat", and "MC_flat_nodiurnal" are 0.54, 0.62, and 0.72, respectively. Because the presence of the MC islands is the sole difference between the "Control" and "MC" experiments, the difference in their ratios (0.35; 0.89 versus 0.54) represents the total damping effect exerted by the MC islands on MJO convective precipitation. Similarly, the role of land-atmosphere interactions in the MC barrier effect can be isolated by the difference between the "Control" and "MC_flat" experiments, which yields a damping of 0.27 (0.89 versus 0.62). Furthermore, the specific role of the MC topography can be quantified by the difference between the "MC" and "MC_flat" experiments, which is 0.08 (0.62 versus 0.54). Finally, the contribution of the diurnal cycle can be estimated by the difference between the "MC_flat" and "MC_flat_nodiurnal" experiments, which amounts to 0.10 (0.62 versus 0.72).

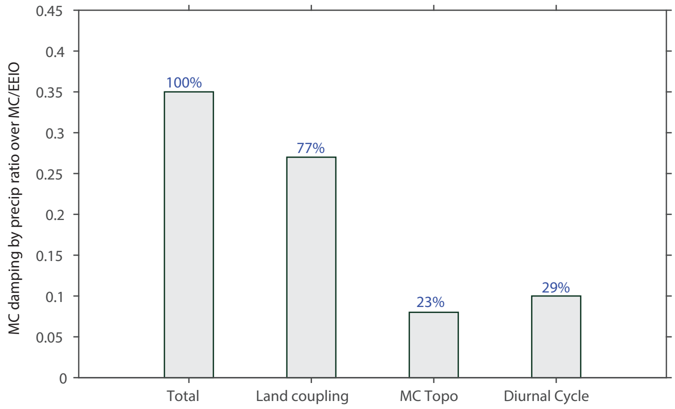

Fig. 4. Relative contributions (blue percentages) of the land-atmosphere interactions, MC topography, and the diurnal cycle to the total damping effect on MJO convection. Values on the y-axis denote the magnitude of damping exerted by each process over the MC region (see text for details).

The relative contributions of land-atmosphere interactions, the MC topography, and the diurnal cycle to the total MC damping effect on MJO convection are summarized in Fig. 4. Of the total MJO damping effect over Sumatra Island in the "MC" experiment, approximately 77% is driven by land-atmosphere interactions, whereas only about 23% is attributable to the MC topography. Although the influence of the MC topography might be underestimated due to the relatively coarse model resolution used in this study, Figure 4 clearly demonstrates a critical role of the land-atmosphere interactions in damping MJO convection over the MC. Furthermore, the results indicate that the diurnal cycle accounts for approximately 29% of the total damping effect, which aligns with findings from previous studies (e.g., Oh et al. 2013; Hagos et al. 2016).

It is important to note that the impact of the diurnal cycle on MJO damping, as shown in Fig. 4, is not independent of the land-atmosphere interactions. Because the systematic eastward-propagating MJO events along the equator remain largely intact across these experiments (see Supporting Fig. S2, alongside Figs. 2b and 2d), this indicates that the reduced MC damping effect simulated in the "MC_flat_nodiurnal" experiment is primarily driven by changes in local land-atmosphere interactions over the MC region, rather than broader domain-wide changes in convective organization. This local interactive mechanism will be further explored below.

3.3 The underlying land-atmosphere coupling processes responsible for the MC barrier effect

By capitalizing on the realistic simulations of the MC barrier effect on the MJO in the "MC_flat" experiment, we now investigate the key land-atmosphere coupling processes responsible for the damping of MJO convection over the MC, with a specific focus on Sumatra.

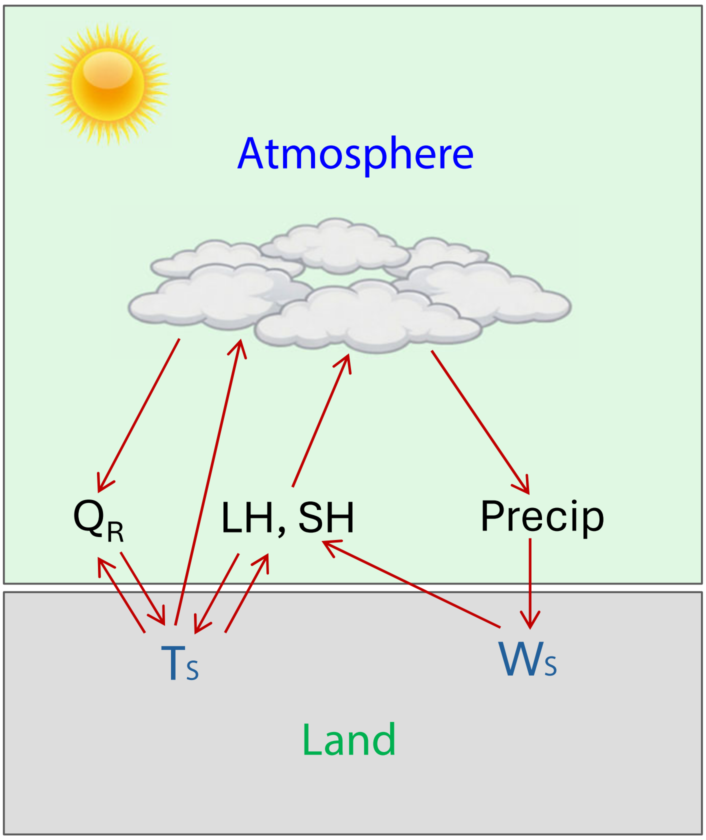

Fig. 5. A schematic depicting the interactive processes between the atmosphere and the land surface in the ECHAM4 GCM. Here, T_S denotes surface temperature, W_S soil moisture, Q_R radiative heat fluxes at the surface, LH and SH surface latent and sensible heat fluxes, and Precip surface precipitation. In ECHAM4, soil moisture is computed based on a one-layer bucket model, with the field capacity varying by soil type.

Atmospheric influences on land properties in the ECHAM4.6 model is primarily governed by land surface processes, specifically through variations in land surface temperature (Ts) and soil moisture (Ws) (see the schematic in Fig. 5). First, Ts is influenced by shortwave and longwave radiative fluxes, along with latent and sensible heat fluxes at the surface. Modulations of Ts, in turn, alter surface radiative and turbulent heat fluxes, thereby modifying the vertical thermodynamic profiles of temperature and moisture. Consequently, these changes in atmospheric stratification modulate convective instability, leading to condensation and associated cloud formation, which feed back onto radiation. Concurrently, variations in soil moisture (Ws)—primarily driven by surface precipitation—impact the partitioning of surface latent and sensible heat fluxes, which in turn influences Ts and associated vertical thermodynamic profiles.

The fact that the MC barrier effect is well captured in the "MC_flat" experiment suggests that, given the presence of MJO convection over the eastern Indian Ocean, changes in Ts and/or Ws driven by atmospheric conditions, and their subsequent feedbacks to the atmosphere, can effectively inhibit the development of MJO convection over the MC. In this section, we conduct additional experiments to determine whether Ts or Ws involved in the land-atmosphere coupling is the primary driver of the MC barrier effect.

First, a new experiment is conducted base on the "MC_flat" setup, but with the land-atmosphere coupling over the MC entirely muted. This is achieved by overriding both the model Ts and Ws with their climatological mean values (derived from the "MC_flat" experiment) at each time step (hereafter, the "MC_flat_nocoupling" experiment). As shown in Fig. 6b, the MC barrier effect completely vanishes when land-atmosphere interactions are muted using this overriding approach; instead, strongly enhanced MJO convection over Sumatra is simulated in the "MC_flat_nocoupling" experiment. This result confirms the crucial role of land-atmosphere coupling in the MC barrier effect.

To further examine the relative roles of Ts and Ws in the land-atmosphere coupling responsible for the MC barrier effect, two additional experiments are conducted by enforcing partial coupling. In the first experiment ("MC_flat_Ts_coupling"), Ts is allowed to freely evolve in response to atmospheric changes, while Ws is overridden with its climatology derived from the "MC_flat" experiment. Conversely, in the second experiment ("MC_flat_Ws_coupling"), Ws freely evolves while Ts is replaced with its climatology from "MC_flat". As shown in Fig. 6, the damping of MJO convection over the MC simulated in "MC_flat" is largely reproduced in the "MC_flat_Ts_coupling" experiment (Fig. 6c). This stands in stark contrast to the strongly enhanced MJO convection over the MC land seen in the "MC_flat_W_S_coupling" experiment (Fig. 6d). Therefore, variations in T_S driven by land-atmosphere interactions play the dominant role in the MC barrier effect on MJO convection.

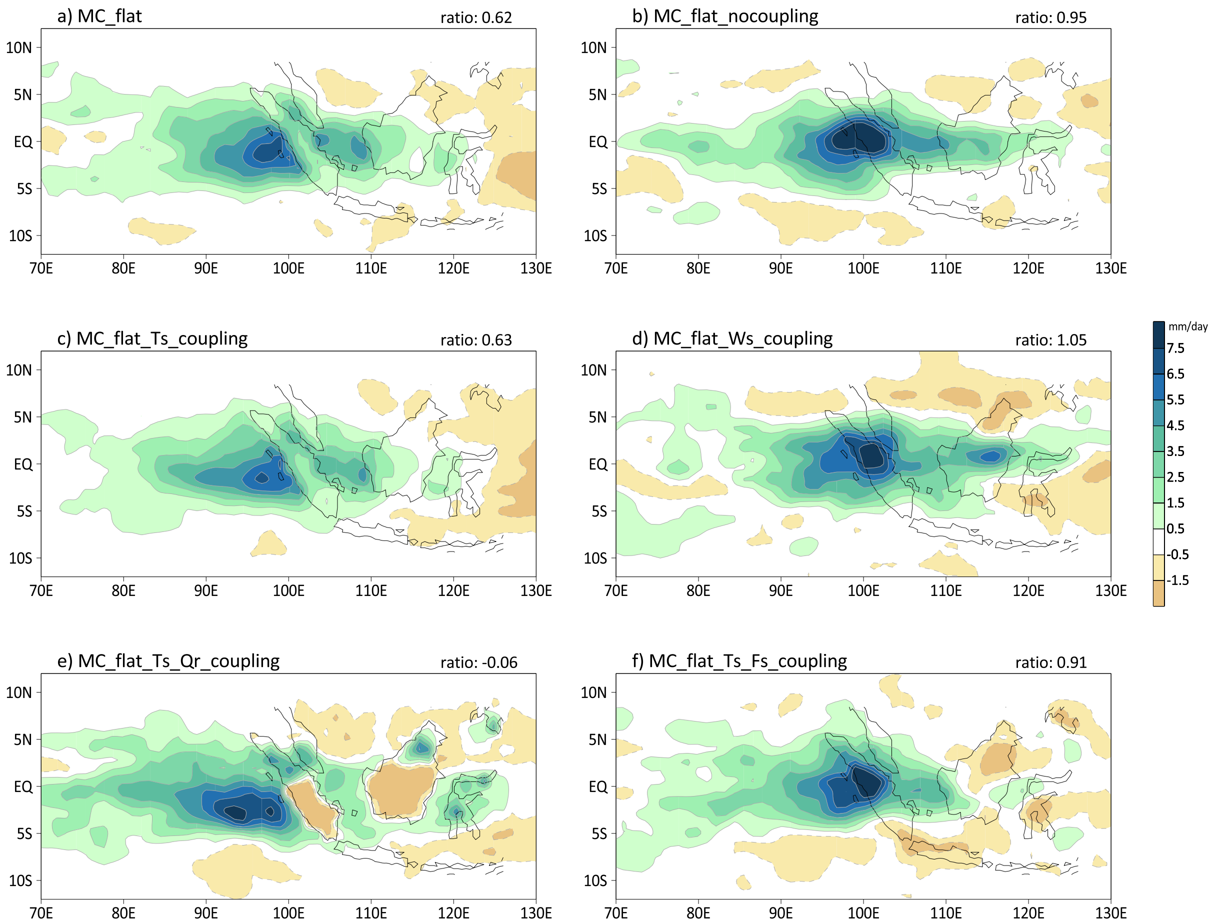

Fig. 6. As in Fig. 3, but for the spatial patterns of convective precipitation anomalies in various model experiments based on the "MC_flat" configuration, including the "MC_flat" (a; duplicated from Fig. 3f), "MC_flat_nocoupling" (b), "MC_flat_T_S_coupling" (c), "MC_flat_W_S_coupling" (d), "MC_flat_T_S_Q_R_coupling" (e), and "MC_flat_T_S_F_S_coupling" (f) experiments. The value displayed in the upper right corner of each panel denotes the corresponding convective precipitation ratio between Sumatra and the MJO convection center over the eastern Indian Ocean. See Table 1 for detailed descriptions of these experiments.

As variations in T_S can be driven by changes in both surface radiative fluxes (Q_R) and turbulent (sensible and latent) heat fluxes (F_S), we conduct two additional experiments based on the "MC_flat_T_S_coupling" setup to determine whether coupling with surface radiation or turbulent heat fluxes is the primary driver of the MC barrier effect. In the first experiment ("MC_flat_T_S_Q_R_coupling"), in addition to overriding W_S, the total surface sensible and latent fluxes (F_S) over the MC are replaced with their climatologies obtained from the "MC_flat" experiment, while Q_R is allowed to freely evolve and couple with T_S. In the second experiment ("MC_flat_Ts_Fs_coupling"), in addition to W_S, Q_R is overridden with its "MC_flat" climatology, while F_S is allowed to freely evolve and couple with T_S.

Results suggest that, concurrent with enhanced MJO convection over the eastern Indian Ocean, radiation-induced T_S changes lead to strongly suppressed convection over a large portion of the MC land, including both Sumatra and Borneo (Fig. 6e). In contrast, the F_S-driven T_S changes lead to strongly enhanced MJO convection over Sumatra (Fig. 6f). It is noteworthy that that these strong negative MJO precipitation anomalies over the MC driven by radiation-induced T_S changes can be partially offset by enhanced MJO convection when allowing W_S (Fig. 6d) and F_S (Fig. 6f) to vary, although non-linear interaction is expected among these complex coupling processes.

These results suggest that the MC barrier effect can be primarily attributed to the land-atmosphere coupling driven by radiation-induced changes in T_S, a mechanism fundamentally captured in the "MC_flat_Ts_QR_coupling" experiment (Fig. 6e). In the following, we conduct detailed diagnostic analyses based on this experiment to further elucidate the key land-atmosphere coupling processes underlying the MC barrier effect.

Alongside the spatial pattern of convective precipitation anomalies from the "MC_flat_Ts_QR_coupling" experiment (Fig. 7a, duplicated from Fig. 6e), Fig. 7b illustrates the corresponding pattern of convective available potential energy (CAPE) anomalies associated with the MJO convection center over the eastern Indian Ocean. Here, CAPE is defined as the vertically integrated buoyancy anomalies above the cloud base and is obtained directly as a model output. It is evident that the anomalous MJO convective precipitation pattern closely mirrors the spatial distribution of CAPE. Specifically, suppressed convection over the MC land, including large portions of Sumatra and Borneo, is closely linked to local negative CAPE anomalies. This robust coupling between convective precipitation and CAPE associated with the MJO is largely consistent with the recently proposed precipitation-buoyancy framework (Ahmed et al. 2020; Adames et al. 2021). This framework is further supported by a largely linear relationship between the unfiltered daily CAPE and convective precipitation, as illustrated in Fig. 7c, which plots composite daily CAPE as a function of daily convective precipitation for both the oceanic and land grids across the Indo-Pacific warm pool (70-150ºE; 10ºS-10ºN). These composite analyses are based on sample sizes of 866,880 for land and 169,920 for oceanic regions, respectively, with a correlation coefficient of approximately 0.98 between CAPE and convective precipitation for both regions.

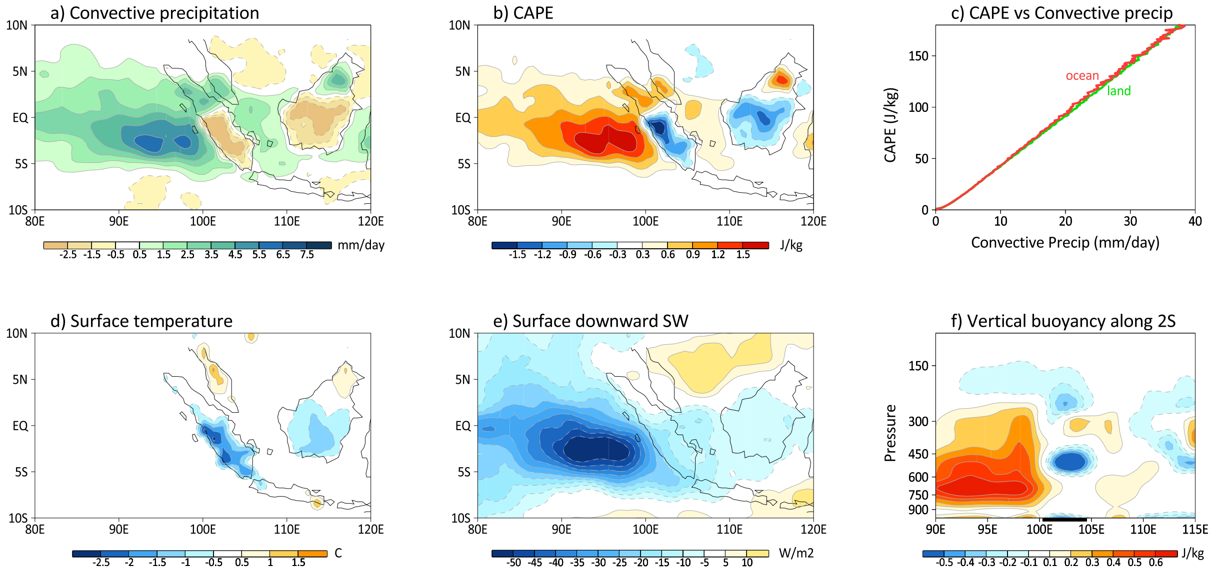

Fig. 7. Processes underlying the weakening of MJO convection over the MC based on the "MC_flat_T_S_Q_R_coupling" experiment. Shown are the spatial patterns of a) anomalous convective precipitation (duplicated from Fig. 6e, but with a different domain size and color scale), b) convective available potential energy (CAPE), defined as the vertically integrated buoyancy above the cloud base, d) surface temperature (T_S), and e) downward short-wave radiative flux at the surface. c) Composite daily CAPE as a function of daily precipitation for both land (green) and oceanic (red) grids over the Indo-Pacific warm pool region (70-150°E; 10°S-10°N). f) A vertical-longitude cross-section of MJO buoyancy anomalies along 2°S, where the strongest MJO damping is simulated, as shown in a). The location of the MC landmass is denoted by the black bar at the bottom of panel f).

Furthermore, Fig. 7d illustrates that the negative CAPE anomalies over the MC land in the "MC_flat_T_S_Q_R_coupling" experiment (Fig. 7b) are closely associated with negative T_S anomalies, which are in turn driven by local reductions in downward surface shortwave radiation (Fig. 7e) acting upon the relatively small heat capacity of the land. This reduction in surface shortwave radiation over the MC land is part of a broader negative anomalous pattern extending across the eastern Indian Ocean and the MC region (Fig. 7e), primarily driven by increased cloudiness associated with enhanced MJO convection (not shown). As further illustrated by the vertical-longitude cross-section of buoyancy at 2°S (Fig. 7f), the surface cooling over the MC landmass induced by this cloud-radiative effect strongly suppresses the buoyancy of rising air parcels and their associated entrainment, ultimately leading to reduced convective precipitation.

3.4 The role of the diurnal cycle in the MC barrier effect

Since the "MC_flat_T_S_Q_R_coupling" experiment captures the essential land-atmosphere coupling processes underlying the MC barrier effect, it offers a unique opportunity to further explore how the diurnal cycle contributes to the suppressed MJO convection over the MC in this simplified case. Motivated by our earlier finding that radiation-induced T_S changes are crucial for the MC barrier effect, Figure 8 presents the diurnal evolution of anomalous convective precipitation, surface downward shortwave radiation, and T_S over the eastern Indian Ocean and MC longitudes along 2°S, based on the "MC_flat_T_S_Q_R_coupling" experiment.

The results indicate that enhanced MJO convective precipitation prevailing over a large area of the eastern Indian Ocean tends to peak around 08 local time (LT, defined by the UTC+7 and applied uniformly across the longitude band; Fig. 8, blue shading). This enhanced precipitation and its associated cloudiness effectively attenuate the downward shortwave radiation over both the eastern Indian Ocean and the MC region, with a maximum reduction occurring near local noon (Fig. 8, red contours). The reduced surface shortwave radiation, acting upon the relatively small heat capacity of the land, in turn leads to strong surface cooling over the MC, with a maximum surface cooling occurring near 14 LT (Fig. 8, blue contours). Since the climatological peak of precipitation over the MC landmass typically occurs during the local afternoon, this anomalous surface cooling peaking around 14 LT − driven by MJO-induced cloud shielding − severely disrupts the thermodynamic destabilization of the boundary layer. Consequently, this generates negative buoyancy anomalies as discussed in Fig. 7, effectively suppressing precipitation over the MC land and leading to a maximum reduction in convective precipitation anomalies around 16 LT (Fig. 8, brown shading).

The results illustrated in Fig. 8 thus suggest that the strong reduction in MJO precipitation over the MC land in the "MC_flat_T_S_Q_R_coupling" experiment is driven by a diurnal phase-locking mechanism resulting from land-atmosphere interactions. Specifically, widespread enhanced MJO precipitation and cloudiness in the local morning substantially reduce downward shortwave radiation, with this reduction peaking at local noon. This midday radiative deficit, in turn, drives strong surface cooling and subsequently weakens convective precipitation over the MC land during the afternoon – precisely when the climatological peak of local diurnal precipitation typically occurs.

It is worth noting that the peak of convective precipitation around 08 LT over the eastern Indian Ocean during the active MJO phase simulated in the "MC_flat_T_S_Q_R_coupling" experiment (Fig. 8) is largely consistent with the early morning precipitation peak (05-08 LT) in observational studies (e.g., Sakaeda et al. 2018; Jiang et al. 2019). A general consistency in the diurnal evolution of total precipitation associated with enhanced MJO convection over the eastern India Ocean between model simulations and GPM IMERG is also illustrated in Supporting Fig. S3 (where results from the experiments "MC" and "MC_flat" are shown to facilitate a more direct comparison to the observations).

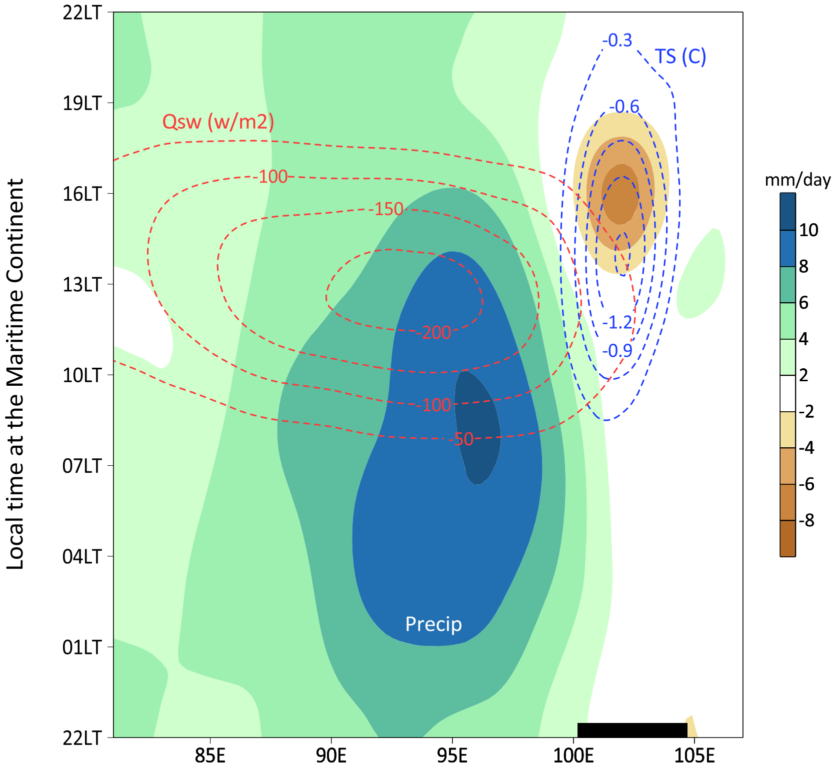

Fig. 8. Diurnal time-longitude evolution of anomalous fields along 2°S associated with MJO convection over the eastern Indian ocean in the "MC_flat_T_S_Q_R_coupling" experiment (as shown in Fig. 7a). Shown are convective precipitation (shading; mm day^{-1}), surface downwelling shortwave radiative fluxes (Q_{SW}, red contours; W m^{-2}), and surface temperature (T_S, blue contours; °C). The diurnal time labelled on the y-axis denotes the local time over the MC region (UTC+7). The location of MC landmass is denoted by the black bar at the bottom of the panel.

When the diurnal cycle is disabled in the model, the aforementioned land-atmosphere interactive processes are expected to weaken substantially, thereby leading to a diminished MC damping effect, as previously demonstrated in the experiment "MC_flat_nodiurnal" (Fig. 3). This is further corroborated by an additional sensitivity experiment based on the "MC_flat_T_S_Q_R_coupling" setup, but with the diurnal cycle of radiation explicitly disabled ("MC_flat_T_S_Q_R_coupling_nodiurnal"). In this case, although the overall damping of MJO convection over the MC land is still evident, the strong negative MJO precipitation anomalies over the MC land simulated in "MC_flat_T_S_Q_R_coupling" are no longer discernible in the absence of the diurnal cycle. Instead, they are replaced by nearly neutral or weakly positive precipitation anomalies (Supporting Figure S4).

4. Summary and Discussions

The MJO serves as an important source of predictability for subseasonal-to-seasonal predictions of climate and weather extremes across the globe. However, the predictive skill of the MJO in current Earth system models is often limited due to various model shortcomings, including challenges in accurately representing the propagation of the MJO over the MC. Meanwhile, the key interactive processes between the MJO and the MC landmasses that contribute to the damping of MJO convection over the MC − known as the MC barrier effect − remain poorly understood.

In this study, with a particular focus over Sumatra, the key processes underlying the damping effect of the MC islands on the eastward-propagating MJO are investigated based on a series of idealized AGCM simulations, in which realistic MC topography and land-sea distribution are embedded in a global aqua-planet environment. By capitalizing on realistic simulations of the observed MC damping effect on the MJO in a base experiment (the "MC" experiment), additional sensitivity experiments suggest that the topography over the MC plays only a minor role (~23%) in the damping effect. Rather, land-atmosphere coupling through interactions among clouds, radiation, land surface temperature, and convective instability, is found to play the dominant role in damping MJO convection over the MC islands. Among these interactive processes, we find that including the diurnal cycle of convection in the model can significantly enhance this damping effect (~29%) due to a more active interaction between convection and shortwave radiation. Specifically, widespread MJO precipitation and enhanced cloudiness during the local morning substantially reduce downward shortwave radiation, culminating in a midday radiative deficit over the eastern Indian Ocean and neighboring areas. This deficit, in turn, drives strong surface cooling and subsequently weakens convective precipitation over the MC land during the afternoon–precisely when the climatological peak of local diurnal precipitation typically occurs. The enhancement of the MC barrier effect on MJO convection by the diurnal cycle is consistent with findings from previous modeling studies.

Importantly, while the critical role of land-atmosphere interactions in the MC barrier effect is clearly illustrated by these idealized model simulations, the impact of MC mountain topography–including associated local circulations such as land-sea breezes–on the MJO may be underestimated due to the relatively coarse resolution of the AGCM used in this study. Additionally, the results in this study are derived from idealized aqua-planet simulations forced by a zonally uniform SST pattern, which excludes the influences of the Indo-Pacific warm pool base state on MJO propagation over the MC. In reality, east-west shifts of the Indo-Pacific warm pool, such as those associated with the El Niño-Southern Oscillation (ENSO), can significantly affect MJO propagation over the MC region (e.g., Gonzalez and Jiang 2017). Notably, these large-scale background patterns can also modulate the local land-atmosphere interactive processes identified here. For example, while a positive ENSO condition tends to favor the continuous eastward propagation of the MJO across the MC (Gonzalez and Jiang, 2017; DeMott et al., 2018), its induced large-scale suppressed convection over the region could simultaneously enhance the local diurnal cycle, thereby amplifying the local damping effect on the MJO. Furthermore, the representation of the MC barrier effect on MJO convection could be sensitive to the model's cumulus parameterization schemes. Therefore, the specific percentages quantifying the MC damping effect (e.g., the ~23% topographic contribution and ~29% diurnal enhancement) should only be interpreted as valuable mechanistic insights rather than universal quantitative estimates.

Despite these caveats, the findings from this study offer crucial implications for the modeling community to improve the simulation of MJO propagation over the MC. Given that the aforementioned land-atmosphere coupling processes largely dictate the MC barrier effect, modeling efforts must prioritize the accurate representation of the diurnal phase relationship between MJO-induced convective cloudiness and surface downwelling shortwave radiation. This requires improvements in cloud schemes to accurately simulate cloud optical properties and their diurnal lifecycle over land. Furthermore, land surface models must correctly capture the rapid response of land surface temperature (Ts) to these radiative flux changes, which hinges on the accurate depiction of soil processes and surface heat capacity. Simultaneously, cumulus parameterizations need to accurately translate these Ts fluctuations—and the associated variations in vertical thermodynamic stratification and buoyancy—into the appropriate convective response. Finally, even with a realistic representation of diabatic heating, the model's dynamical core must properly depict the subsequent circulation responses over the MC region, a task that would benefit greatly from high-resolution topography. Collectively, these tightly coupled processes represent a grand challenge for current climate models. Future studies are warranted to validate the mechanisms underlying the MC damping effect using high-resolution observations and models with either parameterized or explicitly resolved cumulus convection. Ultimately, these future investigations will help us to better understand how local processes, including the land-atmosphere interactions emphasized here, as well as ocean-atmosphere interactions, coordinate with the large-scale Indo-Pacific warm pool variability in affecting MJO propagation over the MC region.

Data availability

The GPM IMERG rainfall data (version 7) can be accessed from the website: https://disc.gsfc.nasa.gov/datasets/GPM_3IMERGHH_07/summary.

Acknowledgements

We acknowledge support by the Regional and Global Model Analysis Program of U.S. Department of Energy under Award DE-SC0024315. We thank Dr. Sandro Lubis and two other anonymous reviewers for insightful comments on an earlier version of this manuscript.

References

Abhik, S., H. H. Hendon, and C. Zhang, 2023: The Indo-Pacific Maritime Continent Barrier Effect on MJO Prediction. *J. Clim.*, **36**, https://doi.org/10.1175/JCLI-D-22-0010.1**,** 945-957.

Adames, Á. F. and J. M. Wallace, 2015: Three-Dimensional Structure and Evolution of the Moisture Field in the MJO. *J. Atmos. Sci.*, **72**, doi:10.1175/JAS-D-15-0003.1**,** 3733-3754.

Adames, Á. F. and E. D. Maloney, 2021: Moisture Mode Theory's Contribution to Advances in our Understanding of the Madden-Julian Oscillation and Other Tropical Disturbances. *Current Climate Change Reports*, 10.1007/s40641-021-00172-4.

Adames, Á. F., S. W. Powell, F. Ahmed, V. C. Mayta, and J. D. Neelin, 2021: Tropical Precipitation Evolution in a Buoyancy-Budget Framework. *J. Atmos. Sci.*, **78**, 10.1175/jas-d-20-0074.1**,** 509-528.

Ahmed, F., n. F. Adames, and J. D. Neelin, 2020: Deep Convective Adjustment of Temperature and Moisture. *J. Atmos. Sci.*, **77**, 10.1175/jas-d-19-0227.1**,** 2163-2186.

Ahn, M.-S., D. Kim, Y.-G. Ham, and S. Park, 2020a: Role of Maritime Continent Land Convection on the Mean State and MJO Propagation. *J. Clim.*, **33**, 10.1175/jcli-d-19-0342.1**,** 1659-1675.

Ahn, M.-S., D. Kim, D. Kang, J. Lee, K. R. Sperber, P. J. Gleckler, X. Jiang, Y.-G. Ham, and H. Kim, 2020b: MJO Propagation Across the Maritime Continent: Are CMIP6 Models Better Than CMIP5 Models? *Geophys. Res. Lett.*, **47**, 10.1029/2020GL087250**,** e2020GL087250.

Andersen, J. A. and Z. Kuang, 2012: Moist Static Energy Budget of MJO-like Disturbances in the Atmosphere of a Zonally Symmetric Aquaplanet. *J. Clim.*, **25**, 10.1175/jcli-d-11-00168.1**,** 2782-2804.

Balmaseda, M. A., A. Barros, S. Hagos, B. Kirtman, H.-Y. Ma, Y. Ming, A. Pendergrass, V. Tallapragada, and E. Thompson, 2020: "NOAA-DOE Precipitation Processes and Predictability Workshop." U.S. Department of Energy and U.S. Department of Commerce NOAA; DOE/SC-0203; NOAA Technical Report OAR CPO-9.

Baranowski, D. B., D. E. Waliser, X. Jiang, J. A. Ridout, and M. K. Flatau, 2019: Contemporary GCM Fidelity in Representing the Diurnal Cycle of Precipitation Over the Maritime Continent. *Journal of Geophysical Research: Atmospheres*, **124**, 10.1029/2018JD029474**,** 747-769.

Birch, C. E., S. Webster, S. C. Peatman, D. J. Parker, A. J. Matthews, Y. Li, and M. E. E. Hassim, 2016: Scale Interactions between the MJO and the Western Maritime Continent. *J. Clim.*, **29**, doi:10.1175/JCLI-D-15-0557.1**,** 2471-2492.

Chikira, M., 2014: Eastward-Propagating Intraseasonal Oscillation Represented by Chikira–Sugiyama Cumulus Parameterization. Part II: Understanding Moisture Variation under Weak Temperature Gradient Balance. *J. Atmos. Sci.*, **71**, 10.1175/JAS-D-13-038.1**,** 615-639.

DeMott, C. A., B. O. Wolding, E. D. Maloney, and D. A. Randall, 2018: Atmospheric Mechanisms for MJO Decay Over the Maritime Continent. *Journal of Geophysical Research: Atmospheres*, **123**, 10.1029/2017jd026979**,** 5188-5204.

Feng, J., T. Li, and W. Zhu, 2015: Propagating and Nonpropagating MJO Events over Maritime Continent. *J. Clim.*, **28**, 10.1175/JCLI-D-15-0085.1**,** 8430-8449.

Gonzalez, A. O. and X. Jiang, 2017: Winter Mean Lower-Tropospheric Moisture over the Maritime Continent as a Climate Model Diagnostic Metric for the Propagation of the Madden-Julian Oscillation. *Geophys. Res. Lett.*, 10.1002/2016GL072430.

——, 2019: Distinct Propagation Characteristics of Intraseasonal Variability Over the Tropical West Pacific. *Journal of Geophysical Research: Atmospheres*, **0**, 10.1029/2018JD029884.

Hagos, S. M., C. Zhang, Z. Feng, C. D. Burleyson, C. De Mott, B. Kerns, J. J. Benedict, and M. N. Martini, 2016: The impact of the diurnal cycle on the propagation of Madden-Julian Oscillation convection across the Maritime Continent. *Journal of Advances in Modeling Earth Systems*, 10.1002/2016MS000725.

Hsu, H.-H. and M.-Y. Lee, 2005: Topographic Effects on the Eastward Propagation and Initiation of the Madden–Julian Oscillation. *J. Clim.*, **18**, doi:10.1175/JCLI-3292.1**,** 795-809.

Huffman, G., D. T. Bolvin, E. J. Nelkin, and J. Tan, 2019: Integrated Multi-Satellite Retrievals for GPM (IMERG) technical documentation. NASA Tech. Doc., 77 pp.

Hung, C.-S. and C.-H. Sui, 2018: A Diagnostic Study of the Evolution of the MJO from Indian Ocean to Maritime Continent: Wave Dynamics versus Advective Moistening Processes. *J. Clim.*, **31**, 10.1175/jcli-d-17-0139.1**,** 4095-4115.

Inness, P. M. and J. M. Slingo, 2006: The interaction of the Madden-Julian Oscillation with the Maritime Continent in a GCM. *Quart. J. Roy. Meteor. Soc.*, **132,** 1645-1667.

Jiang, X., 2017: Key processes for the eastward propagation of the Madden-Julian Oscillation based on multimodel simulations. *Journal of Geophysical Research: Atmospheres*, 10.1002/2016JD025955.

Jiang, X., H. Su, and D. E. Waliser, 2019: A Damping Effect of the Maritime Continent for the Madden-Julian Oscillation. *Journal of Geophysical Research: Atmospheres*, **124**, 10.1029/2019JD031503**,** 13693-13713.

Jiang, X., E. Maloney, and H. Su, 2020a: Large-scale controls of propagation of the Madden-Julian Oscillation. *npj Climate and Atmospheric Science*, **3**, 10.1038/s41612-020-00134-x**,** 29.

Jiang, X., Á. F. Adames, D. Kim, E. D. Maloney, H. Lin, H. Kim, C. Zhang, C. A. DeMott, and N. P. Klingaman, 2020b: Fifty Years of Research on the Madden-Julian Oscillation: Recent Progress, Challenges, and Perspectives. *Journal of Geophysical Research: Atmospheres*, **125**, 10.1029/2019JD030911**,** e2019JD030911.

Jiang, X., et al., 2015: Vertical structure and physical processes of the Madden-Julian oscillation: Exploring key model physics in climate simulations. *Journal of Geophysical Research: Atmospheres*, **120**, 10.1002/2014JD022375**,** 4718-4748.

Kerns, B. W. and S. S. Chen, 2020: A 20-Year Climatology of Madden-Julian Oscillation Convection: Large-Scale Precipitation Tracking From TRMM-GPM Rainfall. *Journal of Geophysical Research: Atmospheres*, **125**, https://doi.org/10.1029/2019JD032142**,** e2019JD032142.

Kim, D., A. H. Sobel, and I.-S. Kang, 2011: A mechanism denial study on the Madden-Julian Oscillation. *Journal of Advances in Modeling Earth Systems*, **3**, 10.1029/2011MS000081**,** n/a-n/a.

Kim, D., J.-S. Kug, and A. H. Sobel, 2014: Propagating versus Nonpropagating Madden–Julian Oscillation Events. *J. Clim.*, **27**, 10.1175/JCLI-D-13-00084.1**,** 111-125.

Kim, D., H. Kim, and M.-I. Lee, 2017: Why does the MJO detour the Maritime Continent during austral summer? *Geophys. Res. Lett.*, 10.1002/2017GL072643**,** n/a-n/a.

Kim, D., E. Maloney, and C. Zhang, 2020: Review: MJO propagation over the Maritime Continent. The Multiscale Global Monsoon System, C. P. Chang et al., Eds., Vol. 11, World Scientific Series on Asia-Pacific Weather and Climate, World Scientific.

Kim, H.-M., 2017: The Impact of the Mean Moisture Bias on the Key Physics of MJO Propagation in the ECMWF Reforecast. *Journal of Geophysical Research: Atmospheres*, 10.1002/2017JD027005**,** 2017JD027005.

Kim, H., M. A. Janiga, and K. Pegion, 2019: MJO Propagation Processes and Mean Biases in the SubX and S2S Reforecasts. *Journal of Geophysical Research: Atmospheres*, **124**, 10.1029/2019JD031139**,** 9314-9331.

Lee, J.-E., B. R. Lintner, J. D. Neelin, X. Jiang, P. Gentine, C. K. Boyce, J. B. Fisher, J. T. Perron, T. L. Kubar, J. Lee, and J. Worden, 2012: Reduction of tropical land region precipitation variability via transpiration. *Geophys. Res. Lett.*, **39**, 10.1029/2012GL053417**,** n/a-n/a.

Lim, Y., S.-W. Son, and D. Kim, 2018: MJO Prediction Skill of the Subseasonal-to-Seasonal Prediction Models. *J. Clim.*, **31**, 10.1175/JCLI-D-17-0545.1**,** 4075-4094.

Ling, J., C. Zhang, R. Joyce, P.-p. Xie, and G. Chen, 2019: Possible Role of the Diurnal Cycle in Land Convection in the Barrier Effect on the MJO by the Maritime Continent. *Geophys. Res. Lett.*, **46**, 10.1029/2019gl081962**,** 3001-3011.

Lubis, S. W., S. Hagos, C.-C. Chang, K. Balaguru, and L. R. Leung, 2023: Cross-Equatorial Surges Boost MJO's Southward Detour Over the Maritime Continent. *Geophys. Res. Lett.*, **50**, https://doi.org/10.1029/2023GL104770**,** e2023GL104770.

Majda, A. J. and Q. Yang, 2016: A Multiscale Model for the Intraseasonal Impact of the Diurnal Cycle over the Maritime Continent on the Madden–Julian Oscillation. *J. Atmos. Sci.*, **73**, doi:10.1175/JAS-D-15-0158.1**,** 579-604.

Maloney, E. D., 2009: The Moist Static Energy Budget of a Composite Tropical Intraseasonal Oscillation in a Climate Model. *J. Clim.*, **22,** 711-729.

Maloney, E. D. and A. H. Sobel, 2004: Surface Fluxes and Ocean Coupling in the Tropical Intraseasonal Oscillation. *J. Clim.*, **17,** 4368-4386.

Manabe, S., 1969: Climate and the ocean circulation: I. The atmospheric circulation and the hydrology of the Earth's surface. *Mon. Weather Rev.*, **97**, https://doi.org/10.1175/1520-0493(1969)097<0739:CATOC>2.3.CO;2**,** 739-774.

Merryfield, W. J., et al., 2020: Current and Emerging Developments in Subseasonal to Decadal Prediction. *Bull. Am. Meteorol. Soc.*, **101**, 10.1175/bams-d-19-0037.1**,** E869-E896.

Moncrieff, M. W., D. E. Waliser, M. J. Miller, M. A. Shapiro, G. R. Asrar, and J. Caughey, 2012: Multiscale Convective Organization and the YOTC Virtual Global Field Campaign. *Bull. Am. Meteorol. Soc.*, **93**, 10.1175/bams-d-11-00233.1**,** 1171-1187.

Najarian, H., J. Ruppert, and N. Sakaeda, 2025: The Influence of Cloud-Radiative Interactions on the Diurnal Cycle Over the Maritime Continent. *Journal of Geophysical Research: Atmospheres*, **130**, https://doi.org/10.1029/2025JD044512**,** e2025JD044512.

Neale, R. and J. Slingo, 2003: The Maritime Continent and Its Role in the Global Climate: A GCM Study. *J. Clim.*, **16**, 10.1175/1520-0442(2003)016<0834:TMCAIR>2.0.CO;2**,** 834-848.

Neale, R. B. and B. J. Hoskins, 2000: A standard test for AGCMs including their physical parametrizations: I: the proposal. *Atmospheric Science Letters*, **1**, 10.1006/asle.2000.0022, 101-107.

Neena, J. M., J. Y. Lee, D. Waliser, B. Wang, and X. Jiang, 2014: Predictability of the Madden–Julian Oscillation in the Intraseasonal Variability Hindcast Experiment (ISVHE). *J. Clim.*, **27**, 10.1175/JCLI-D-13-00624.1, 4531-4543.

Nordeng, T. E., 1994: Extended versions of the convective parametrization scheme at ECMWF and their impact on the mean and transient activity of the model in the tropics. ECMWF Tech. Memo. 206, 41 pp.

Oh, J.-H., B.-M. Kim, K.-Y. Kim, H.-J. Song, and G.-H. Lim, 2013: The impact of the diurnal cycle on the MJO over the Maritime Continent: a modeling study assimilating TRMM rain rate into global analysis. *Climate Dyn.*, **40**, 10.1007/s00382-012-1419-8, 893-911.

Oh, J. H., K. Y. Kim, and G. H. Lim, 2012: Impact of MJO on the diurnal cycle of rainfall over the western Maritime Continent in the austral summer. *Climate Dyn.*, **38**, DOI 10.1007/s00382-011-1237-4, 1167-1180.

Peatman, S. C., A. J. Matthews, and D. P. Stevens, 2015: Propagation of the Madden–Julian Oscillation and scale interaction with the diurnal cycle in a high-resolution GCM. *Climate Dyn.*, **45**, 10.1007/s00382-015-2513-5, 2901-2918.

Pegion, K., et al., 2019: The Subseasonal Experiment (SubX): A Multimodel Subseasonal Prediction Experiment. *Bull. Am. Meteorol. Soc.*, **100**, 10.1175/bams-d-18-0270.1, 2043-2060.

Roeckner, E., K. Arpe, L. Bengtsson, M. Christoph, M. Claussen, L. Dümenil, M. Esch, M. A. Giorgetta, U. Schlese, and U. Schulzweida, 1996: The atmospheric general circulation model ECHAM-4: Model description and simulation of present-day climate.

Sakaeda, N., S. W. Powell, J. Dias, and G. N. Kiladis, 2018: The Diurnal Variability of Precipitating Cloud Populations during DYNAMO. *J. Atmos. Sci.*, **75**, https://doi.org/10.1175/JAS-D-17-0312.1, 1307-1326.

Salby, M. L. and H. H. Hendon, 1994: Intraseasonal Behavior of Clouds, Temperature, and Motion in the Tropics. *J. Atmos. Sci.*, **51,** 2207-2224.

Sobel, A., S. Wang, and D. Kim, 2014: Moist Static Energy Budget of the MJO during DYNAMO. *J. Atmos. Sci.*, **71**, 10.1175/JAS-D-14-0052.1, 4276-4291.

Sobel, A. H., E. D. Maloney, G. Bellon, and D. M. Frierson, 2008: The role of surface heat fluxes in tropical intraseasonal oscillations. *Nature Geoscience*, **1**, Doi 10.1038/Ngeo312, 653-657.

Sobel, A. H., E. D. Maloney, G. Bellon, and D. M. Frierson, 2010: Surface Fluxes and Tropical Intraseasonal Variability: a Reassessment. *Journal of Advances in Modeling Earth Systems*, **2**, 10.3894/JAMES.2010.2.2, 2.

Tiedtke, M., 1989: A Comprehensive Mass Flux Scheme for Cumulus Parameterization in Large-Scale Models. *Mon. Weather Rev.*, **117,** 1779-1800.

Vitart, F., 2016: MJO prediction Intercomparison using the S2S Database. *International Workshop on the Madden-Julian Oscillation*.

Wang, B. and T. M. Li, 1994: Convective Interaction with Boundary-Layer Dynamics in the Development of a Tropical Intraseasonal System. *J. Atmos. Sci.*, **51,** 1386-1400.

Wang, J., H. Kim, D. Kim, S. A. Henderson, C. Stan, and E. D. Maloney, 2020: MJO Teleconnections over the PNA Region in Climate Models. Part I: Performance- and Process-Based Skill Metrics. *J. Clim.*, **33**, 10.1175/jcli-d-19-0253.1, 1051-1067.

Wu, C.-H. and H.-H. Hsu, 2009: Topographic Influence on the MJO in the Maritime Continent. *J. Clim.*, **22**, doi:10.1175/2009JCLI2825.1, 5433-5448.

Xavier, P., S. Y. Lim, M. F. Ammar Bin Abdullah, M. Bala, S. N. Chenoli, A. S. Handayani, C. Marzin, D. Permana, F. Tangang, K. D. Williams, and D. J. Yik, 2020: Seasonal Dependence of Cold Surges and their Interaction with the Madden–Julian Oscillation over Southeast Asia. *J. Clim.*, **33**, https://doi.org/10.1175/JCLI-D-19-0048.1, 2467-2482.

Yoneyama, K. and C. Zhang, 2020: Years of the Maritime Continent. *Geophys. Res. Lett.*, **47**, 10.1029/2020GL087182, e2020GL087182.

Yoneyama, K., C. Zhang, and C. N. Long, 2013: Tracking Pulses of the Madden–Julian Oscillation. *Bull. Am. Meteorol. Soc.*, **94**, 10.1175/BAMS-D-12-00157.1, 1871-1891.

Zhang, C. and H. H. Hendon, 1997: Propagating and Standing Components of the Intraseasonal Oscillationin Tropical Convection. *J. Atmos. Sci.*, **54**, doi:10.1175/1520-0469(1997)054<0741:PASCOT>2.0.CO;2, 741-752.

Zhang, C. and J. Ling, 2017: Barrier Effect of the Indo-Pacific Maritime Continent on the MJO: Perspectives from Tracking MJO Precipitation. *J. Clim.*, **30**, 10.1175/JCLI-D-16-0614.1, 3439-3459.